

Least-squares analysis of overlapped bound-free absorption spectra and predissociation data in diatomics: The $C(^1\Pi_u)$ state of I_2

Cite as: J. Chem. Phys. **135**, 054301 (2011); <https://doi.org/10.1063/1.3616039>

Submitted: 08 April 2011 . Accepted: 05 July 2011 . Published Online: 01 August 2011

Joel Tellinghuisen



View Online



Export Citation

ARTICLES YOU MAY BE INTERESTED IN

Iodine Revisited

The Journal of Chemical Physics **55**, 288 (1971); <https://doi.org/10.1063/1.1675521>

Resolution of the visible-infrared absorption spectrum of I_2 into three contributing transitions

The Journal of Chemical Physics **58**, 2821 (1973); <https://doi.org/10.1063/1.1679584>

Transition strengths in the visible-infrared absorption spectrum of I_2

The Journal of Chemical Physics **76**, 4736 (1982); <https://doi.org/10.1063/1.442791>

Lock-in Amplifiers up to 600 MHz

starting at

\$6,210



Zurich
Instruments

Watch the Video



Least-squares analysis of overlapped bound-free absorption spectra and predissociation data in diatomics: The $C(^1\Pi_u)$ state of I_2

Joel Tellinghuisen^{a)}

Department of Chemistry, Vanderbilt University, Nashville, Tennessee 37235, USA

(Received 8 April 2011; accepted 5 July 2011; published online 1 August 2011)

Absorption spectra are recorded at low resolution but high quantitative precision for I_2 vapor at 35 °C and 64 °C. These and literature spectra are analyzed by least-squares quantum spectral simulation of the overlapped $A \leftarrow X$, $B \leftarrow X$, and $C(^1\Pi_u) \leftarrow X$ transitions, with the aid of a pseudocontinuum model for the discrete regions of the $A \leftarrow X$ and $B \leftarrow X$ spectra. The analysis yields improved descriptions of the small- R regions of the A - and B -state potentials, which are known precisely at larger R from discrete spectroscopy. The C potential is determined at small R from its $C \leftarrow X$ absorption, at intermediate R from literature data for $B \rightarrow C$ predissociation, and at large R from its known van der Waals well. The estimates of the electronic transition moment function $|\mu_e(R)|$ for the $B \leftarrow X$ transition expand upon precise results from a recent determination by a different method. For the $C \leftarrow X$ and $A \leftarrow X$ transitions, the R -dependence of the transition moment functions resembles that found previously for these systems in Br_2 . Of the spectroscopic properties, the $C \leftarrow X$ spectrum is most altered from the previous analysis, being now $\sim 20\%$ weaker. For $B \rightarrow C$ predissociation, no derived C potential has yielded computed rates in adequate statistical agreement with the analyzed experimental data.

© 2011 American Institute of Physics. [doi:10.1063/1.3616039]

I. INTRODUCTION

The visible absorption spectrum of I_2 is comprised of three overlapped electronic transitions— $B\ 0_u^+(^3\Pi) \leftarrow X\ 1\ \sum_g^+$, $A\ 1_u(^3\Pi) \leftarrow X$, and $C\ 1_u(^1\Pi) \leftarrow X$.^{1,2} The first of these is responsible for most of the absorption and all of the discrete line structure for $\lambda < 800$ nm. It is known with remarkable breadth and precision, some 10^5 assigned lines having been measured to $\sim 10^{-3}$ cm^{-1} , sampling vibrational levels to within 2 cm^{-1} of the B -state dissociation limit. Complementary fluorescence studies have characterized the X state with similar precision to within 5 cm^{-1} of its limit.^{3,4} Through a modest number of spectroscopic constants, the assigned lines can be reproduced within ~ 0.002 cm^{-1} , and even better than this in some regions.⁵ The weakly bound A state has recently been analyzed with comparable precision over $>90\%$ of its well depth.^{6,7} The C state is only very weakly bound,⁸ but its van der Waals potential well is now well described.⁹ However, at room temperature the $C \leftarrow X$ absorption is entirely bound-free and $A \leftarrow X$ almost so. The dominant $B \leftarrow X$ absorption is also bound-free for $\lambda < 500$ nm. Resolution of the spectrum into these three component bands has been a target of quantitative analysis in the past, the current interpretation being as summarized in Fig. 1.^{2,10}

This figure reveals the main challenge to such an analysis: While the $A \leftarrow X$ band appears clearly as a shoulder at long wavelength, the $B \leftarrow X$ and $C \leftarrow X$ bands share the main peak, with no obvious evidence of two transitions. Previous attempts to resolve this band have focused on estimating the

strength of the weaker $C \leftarrow X$ system — from continuous absorption between the lines of the $B \leftarrow X$ system in its fully discrete region ($\lambda > 520$ nm),^{10–12} from photodissociation $I^*(^2P_{1/2})$ to $I(^2P_{3/2})$ branching ratios for $\lambda < 500$ nm,^{13,14} and from the properties of the $I^* \rightarrow I$ photodissociation atomic laser.¹⁵ The $C \leftarrow X$ bound-free spectrum was computed in trial-and-error fashion to match these estimates and deduce the C potential curve, and the remaining absorption was allocated to $B \leftarrow X$ and used to estimate the R -dependence of this system's electronic transition strength $|\mu_e(R)|^2$ in its continuum.¹⁰ However, a recent analysis of the I_2 absorption spectrum in the 520–640-nm region by least-squares spectral simulation has yielded more precise estimates of both $|\mu_e(R)|$ for $B \leftarrow X$ and the molar absorptivity ϵ_c for $A \leftarrow X + C \leftarrow X$,¹⁶ from which the $C \leftarrow X$ system is found to be $\sim 20\%$ weaker than previously thought and hence in need of a refined analysis. That refinement and the overall better description of the C potential are the main goals of the present contribution.

An alternative approach for band component analysis was demonstrated long ago by Le Roy *et al.*,¹⁷ in a landmark global least-squares (LS) analysis of low-resolution Br_2 absorption spectra recorded at four temperatures from 25 °C to 440 °C by Passchier *et al.*¹⁸ Le Roy's method utilized quantum calculation of the bound-free absorption spectra, with the adjustable LS parameters used to describe the small- R extensions of the potentials and the R -dependent transition moment functions. Burkholder and Bair used Le Roy's program to carry out a similar analysis of the Cl_2 absorption spectrum.¹⁹ Both analyses were limited to truly bound-free $C \leftarrow X$ and $B \leftarrow X$ absorption. This is a minor limitation for Cl_2 , because discrete $B \leftarrow X$ absorption is very weak; but for Br_2 it meant ignoring the roughly 1/4 of the

^{a)} Author to whom correspondence should be addressed. Electronic mail: joel.tellinghuisen@vanderbilt.edu.

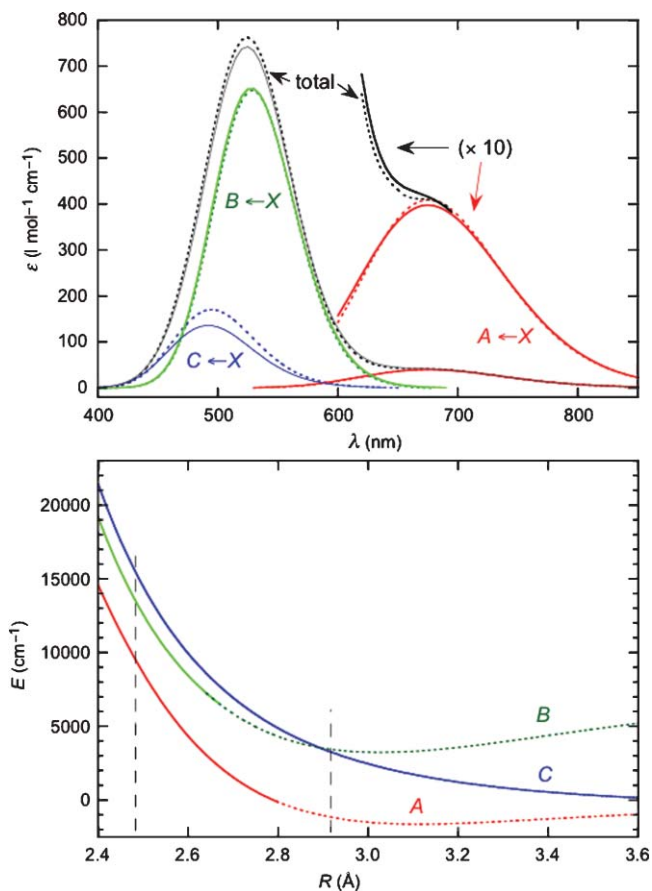


FIG. 1. Visible absorption spectrum (molar absorptivity) of gaseous I_2 near room temperature, with component bands (top), and potential diagram relevant to the absorption. In the spectra, broken curves illustrate results from Ref. 10, while solid curves are current results. In the potential diagram, broken curves illustrate regions known from discrete spectroscopy, and vertical dashed lines delimit absorption region. Energies are relative to lowest dissociation limit. Spectra are computed using the pseudocontinuum model.

absorption that occurs at $\lambda > 500$ nm, where discrete $B \leftarrow X$ absorption begins. I reanalyzed the Br_2 absorption a few years ago,²⁰ extending the spectral coverage to the range 320–675 nm and including the $A \leftarrow X$ band for the first time. To incorporate the discrete $B \leftarrow X$ region in this analysis, I used a pseudocontinuum model for the B state, accomplished by artificially making its potential curve extrapolate to dissociation from the B -state minimum. This model is based on the recognition that the Franck-Condon intensity properties of such reflection-type spectra, where the absorption is confined to the upper state's repulsive wall, are determined entirely by the shape of that wall and are completely insensitive to the nature of the attractive branch.^{21,22}

At first inspection, the I_2 absorption spectrum might seem an unappealing subject for such an analysis, because discrete $B \leftarrow X$ absorption accounts for $\sim 3/4$ of the total. Yet the absorption is completely bound-free for $\lambda < 500$ nm, and for $\lambda > 650$ nm it is dominated by the $A \leftarrow X$ transition, which exhibits little structure and little absorption beyond 800 nm, where discrete absorption begins. These factors, combined with the ease with which one can collect abundant accurate and precise absorbance data with modern spectrophotometers, makes such an analysis appear worthwhile. In addition,

for the 520–640-nm region we have the new estimates of total continuous absorption and precise estimates of $|\mu_e(R)|^2$ for $B \leftarrow X$ to constrain the analysis.¹⁶ Further, with care I am able to include the low-resolution total ϵ measurements in the 600–650-nm region, where Beer's Law holds to a good approximation, and where the residual $B \leftarrow X$ structure averages to its pseudocontinuous approximation in the low-resolution (1 nm) spectra. The result of the analysis is a new description of these overlapping transitions with precision of determination an order of magnitude better than that of previous attempts. Remarkably, this experimentally simple approach outperforms the most sophisticated methods that have been brought to bear on this problem over the years, and it could have been employed 25 years ago! (It does rely on the assumption of independent absorption in the three transitions, which has needed such methods for verification.²³)

In Secs. II–V, I briefly describe the procedures for collecting the spectra and converting them to molar absorptivities. I then review the theory behind the computational methods. These include, in addition to the LS global analysis of absorption spectral data, the LS fitting of data for the spontaneous predissociation of the B state,²⁴ which has been attributed to the C state and thus can help determine the C potential in the intermediate- R region. For the final analysis, the absorption and predissociation data are fitted together, in a grand global LS fit. The computations are driven by nonlinear LS algorithms that typically converge in fewer than 10 iterations to yield estimates of the parameters and their variance-covariance matrix, from which the spectra, potential curves, transition moments, and their statistical errors can be calculated. The computed uncertainties are compared with the sensitivity of the analysis to minor changes in the model to substantiate the order-of-magnitude improvement in the precision of the resolution over previous attempts.

II. EXPERIMENTAL WORK AND DATA ASSESSMENT

Spectra were recorded on a Shimadzu Model UV-2101PC spectrophotometer (double beam) using procedures similar to those described recently,¹⁶ except at lower resolution (1 and 2 nm) and at 2-nm intervals, from 850 nm down to below 400 nm. As before, the I_2 pressure was controlled by a side tube immersed in water. The temperatures of both the cell and this water bath were monitored by thermistors that had been calibrated (estimated ± 0.02 K) against calibrated Hg thermometers. Spectra were recorded at nominal cell temperatures of 35 °C and 64 °C, for about a dozen I_2 concentrations in a run, under slow-drift conditions for the cooled side tube. This drift amount to -0.2° over the spectrum at the highest initial water temperature of 31 °C; it decreased in magnitude for initial temperatures closer to the ambient room temperature of 23 °C. For the higher cell temperature, the cell thermistor measurements varied by as much as 2 K for different positions of the probe; an approximate average was used in computations (but see below). The variability was smaller at the lower cell temperature, again from the smaller cell-ambient temperature difference. The cell and side-tube temperatures were logged with the spectra as

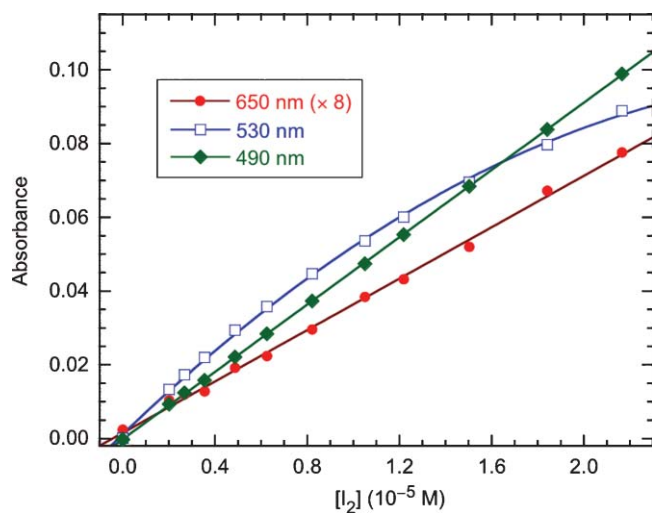


FIG. 2. Absorbance as a function of concentration at selected wavelengths, for a cell at 35 °C having a path length of 9.93(3) cm. The absorption is purely continuous at 490 nm, and mainly discrete at 530 nm; at 650 nm (scaled for display purposes), the absorption is about 80% continuous and 20% from densely overlapped lines of the $B \leftarrow X$ system. The data include blanks at zero concentration. The curves show least-squares fits to straight lines and to a quadratic (530 nm), with intercepts included in both fit models.

functions of time and were later used to compute the concentration for each spectral wavelength.

The $[I_2]$ and absorbance (A) values from all spectra, including baseline spectra ($[I_2] = 0$), were analyzed to obtain estimates of the molar absorptivity. This was done by fitting the A values at each wavelength to linear and quadratic functions of $[I_2]$, with the linear term being the Beer's law quantity, $\varepsilon_\lambda [I_2] \ell$, where ℓ is the path length (see Fig. 2). The quadratic fits were used to identify regions where deviations from Beer's law render the estimates of ε_λ unreliable for use in further analysis. This happens, for example, where the absorption occurs in a few strong, discrete lines (unresolved by the spectrometer) rather than in a true continuum or a pseudo-continuum of densely overlapped discrete lines. In such cases, Beer's law is followed only in the limit of small A , and the absorption drops below the Beer's Law line with increasing optical depth.¹¹ For truly continuous absorption, the quadratic coefficient should be statistically ill-defined, and the linear coefficient from the quadratic fit should agree with that from the linear fit.

Some results of this procedure are illustrated in Fig. 3, showing that Beer's law holds well below 500 nm and above 600 nm, where the two fits yield comparable ε estimates and fit quality. In the region 500–600 nm, where discrete $B \leftarrow X$ absorption dominates, even the quadratic estimate cannot be trusted (with the possible exception of the 575–600 nm region); accordingly the total ε data for this region were omitted from the LS analysis. Experiments like this were run about a dozen times, sometimes with collection of data for only the $\lambda < 500$ nm region, sometimes for only $\lambda > 600$ nm. After examination and comparison, single representative sets of ε values at 35° and at 64 °C, both obtained at 1-nm spectral resolution, were selected for quantitative analysis over the 400–500 and 600–850-nm regions. The σ_ε estimates from the fits, analogous to σ_A in

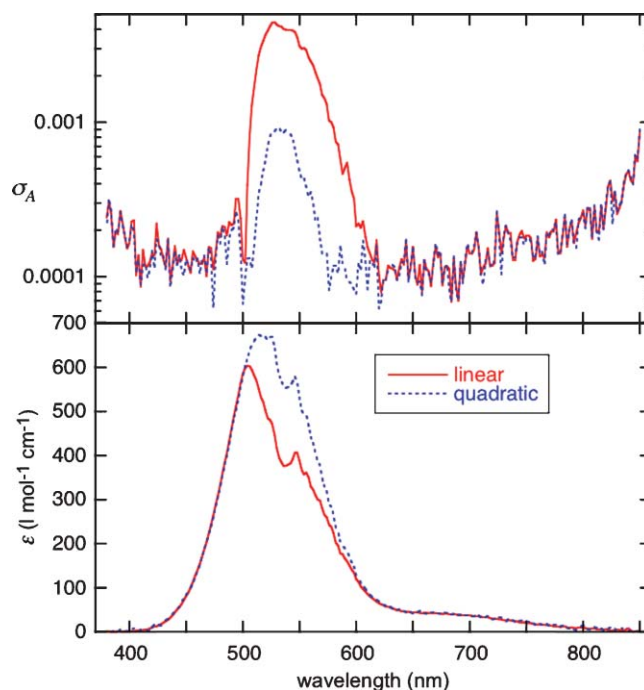


FIG. 3. I₂ molar absorptivity, as estimated from linear and quadratic fits of absorbance data recorded at 2-nm intervals, I₂ pressures 0–400 mTorr, and a cell temperature of 35 °C. The upper panel illustrates the estimated standard deviations from these fits, carried out at each wavelength. Where the linear and quadratic fits diverge in slope, the data are not following Beer's Law; where σ_A rises anomalously (510–580 nm), not even the slope of the quadratic analysis can be trusted as a reliable low- A estimate of ε .

the top part of Fig. 3, were fitted to smooth functions of λ to obtain statistical weights ($1/\sigma_{\varepsilon\lambda}^2$) for the LS analysis.²⁵

Physical limitations of these experiments made it difficult to record spectra reliably for cell temperatures much above the upper value here. Accordingly, to expand the temperature range I included estimates given by Tamres and Bhat at wavelengths between 400 and 500 nm and temperatures of 60°, 90°, and 120°.²⁶ I included in the data set all values for $410 \leq \lambda \leq 495$ nm, omitting the values at 500 nm out of concern for possible “contamination” by discrete absorption (the spectral bandwidth was not given). These were weighted in accord with their stated $2 \text{ l mol}^{-1} \text{ cm}^{-1}$ uncertainty.

Comparison of the present spectra with those of Tamres and Bhat is not straightforward because of the temperature differences. However, my 64 °C spectrum lies $\sim 2\%$ below theirs at 60 °C. Also, they reported an isosbestic point (with respect to temperature) at 480 nm and gave $\varepsilon_{480} = 350 \text{ l mol}^{-1} \text{ cm}^{-1}$; my values there are 333 and 337 $\text{l mol}^{-1} \text{ cm}^{-1}$, as compared with my earlier value 326(10) (Ref. 11) and 340 $\text{l mol}^{-1} \text{ cm}^{-1}$ given by Lang and Strong.²⁷ Anticipating discussion below, some of the differences are likely due to wavelength errors. In this regard, ε changes by 3.5%/nm in this region, and most authors have not reported checks of the wavelength reliability of their instruments. (The present data at 35 °C are fully consistent with my earlier measurements¹¹ for $\lambda < 510$ nm, but those values were much less precise in both magnitude and cell temperature, so were omitted from the present analysis.)

The estimates of $|\mu_e|^2$ for the $B \leftarrow X$ transition and the underlying continuum ε_c from Table II of Ref. 16 were also included in the final LS analysis. The former were weighted as their reciprocal squared errors. For the ε_c values, the stated fit errors were augmented by the estimated $21 \text{ mol}^{-1} \text{ cm}^{-1}$ uncertainty from background imprecision, the two contributions being assumed to add independently to the variance. The first two values (at 520 nm) were omitted, for reasons discussed in Ref. 16. In addition, to deal with already noted questions concerning wavelength reliability, I included a single very precise estimate of ε made from 13 “time-course” runs at 35°C , in which the absorbance was recorded at 1-s intervals for 100 s, for starting cold-tube temperatures between 13°C and 28°C , nominally at 500 nm (500.2 nm with wavelength calibration correction²⁸). This value was $587.4 (8) \text{ l mol}^{-1} \text{ cm}^{-1}$.

In their meticulous study of predissociation in $\text{I}_2(B)$,²⁴ Vigué *et al.* quantitatively characterized hyperfine, rotational, and magnetic predissociation, and attributed all of these processes to interaction with the C state. Their estimates of the coefficients α_v^2 for magnetic predissociation were most extensive (in B -state vibrational level ν_B) and, except for several values for $\nu_B < 7$, most precise. Since all three modes of predissociation have rates proportional to a squared B - C wavefunction overlap integral, I have used just these α_v^2 values (their Table VII) to incorporate $B \rightarrow C$ predissociation in the present analysis. Weights were computed from the reported statistical errors.

Finally, to constrain the C potential at large R , I have included in the fit model 8 left-branch turning points on the Rydberg-Klein-Rees (RKR) curve, for $\nu = 0$ –7.⁹ Plots of $\ln(\text{slope})$ vs. $\ln(R)$ for this branch did not show a ν region of clearly smooth behavior, raising doubts about the appropriateness of the attachment procedure that was employed for the A and B curves (see below). Also, above $\nu = 7$ (which is energetically 60% of dissociation), the RKR curve exhibits the erratic behavior generally attributed to limitations in the rotational constants B_ν in the approach to dissociation.^{29,30} Preliminary fits of the 8 RKR points to the exponential polynomial form used in the fitting (see below) gave an estimated σ_y of 0.6 cm^{-1} , from which weights for these data were taken as 2.7 (treating R as error-free, $U_C(R)$ as uncertain).

III. METHOD OF ANALYSIS

A. Theory summary

The theory of bound-free absorption in diatomics is well established and needs only brief review.^{17,20,22} The absorption cross section from level (ν'', J'') to continuum level at energy ε' is

$$\sigma_{\nu,ab}(\nu'', J'') = \frac{2\pi^2\nu}{3\varepsilon_0hc} G_{ab} |\langle \varepsilon' J'' | \mu_e(R) | \nu'' J'' \rangle|^2, \quad (1)$$

where I have replaced the sum over R , P , (Q) branches by the single Q -branch transition (actual or hypothetical). Here ν is the transition wavenumber, and G_{ab} accounts for electronic degeneracy and is unity for $B \leftarrow X$ ($0 \leftarrow 0$ in Hund's

case c) and 2 for $A \leftarrow X$ and $C \leftarrow X$ (both $1 \leftarrow 0$). For room-temperature absorption, this expression must be averaged over the Boltzmann distribution of absorbing ν'' and J'' levels. Experience has shown that for molecules as heavy as Br_2 and I_2 , the rotational averaging can be accomplished with negligible error using 5 appropriately chosen J'' levels, and with very little error using just the average J'' .^{17,20} Nuclear-spin degeneracy effects average out and can be ignored. The vibrational averaging can accommodate a specified fraction of the absorbing population; I have included the first 10 ν'' levels, which covers $> 99.9\%$ of the population at 120°C . The bound and free wavefunctions needed to compute the matrix element in Eq. (1) are obtained by standard numerical methods that may be considered exact. The potential functions used here are effective potentials including the centrifugal term proportional to $J(J+1)/R^2$. Converting the absorption cross section to decadic molar absorptivity ε_ν and expressing the transition moment function in debye ($1\text{D} = 3.3456 \text{ C m}$), we have

$$\varepsilon_\nu = 108.861\nu G_{ab} [|\langle \varepsilon' J'' | \mu_e(R) | \nu'' J'' \rangle|^2]_{\text{avg}}. \quad (2)$$

Spontaneous predissociation rates are proportional to a squared matrix element like that in Eqs. (1) and (2). Since Vigué *et al.*²⁴ analyzed for J dependence, their results should apply for rotationless potential curves. While the electronic operators differ for the three modes and should even include R^{-2} in the case of rotational predissociation, the integrals accumulate over such a narrow range of R that this dependence may be incorporated in the scaling constant (except possibly for the rotational predissociation²⁴). Thus I represent the predissociation rate coefficients as in Ref. 24,

$$\alpha_\nu^2 = P |\langle \nu_B | \varepsilon_C \rangle|^2, \quad (3)$$

in which the continuum level ε_C in the C state lies at the same energy as level ν_B in the B state.

B. Potential curves

At small R , all three potentials are represented as exponential polynomials,^{17,20}

$$U(z) = A_0 + B_0 \exp(a_1 z + a_2 z^2 + \dots); \quad z \equiv R - R_0, \quad (4)$$

in which R_0 is set near the region of strongest absorption, 2.7 \AA for A and B , but for C is taken as 2.83 \AA , where this potential is particularly well defined by the predissociation data (see below). The a_i are LS adjustable parameters, as are A_0 and B_0 for the C potential. For the A and B states, A_0 and B_0 are set to ensure a smooth join with the known regions of these potentials from discrete spectroscopy at larger R . (This attachment procedure is not used for C , for reasons given above.) Beyond the attachment points, the required potential energy points are obtained by interpolating on the A and B RKR curves, with energy set to zero for $R > R_e$ (the pseudo-continuum model). This removal of the attractive branches of the A and B potentials gives them artificial dissociation limits respectively 1639.9 cm^{-1} below and 3321.8 cm^{-1} above the X -state limit.³¹ The C curve is similarly extrapolated to zero at large R , but in this case by attaching an R^{-n} segment beyond

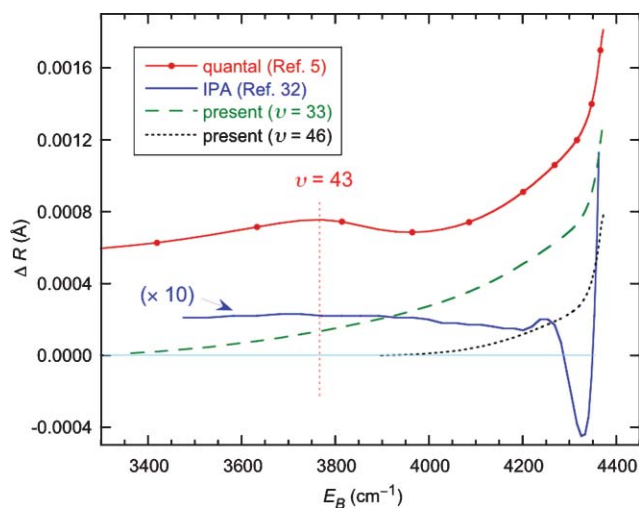


FIG. 4. Effects of various treatments on the repulsive branch of the B -state potential curve. Each R shift is referenced to the RKR potential computed from the constants given in Refs. 3 and 32, as $R(\text{RKR}) - R$. Note the 10-fold magnification of the RKR-IPA differences; the irregular behavior beyond 4200 cm^{-1} is attributable to the RKR curve.

the last fitted RKR point (since Eq. (4) does not go to zero at large z).

The A -state spectroscopic parameters derived in Ref. 7 were near-dissociation expansions for the highest observed levels, and the RKR repulsive branch derived from them behaves smoothly almost to the limit of the analyzed data ($\nu = 35$). In the present analysis, I have used the Ref. 7-based curve up to $\nu = 29$ on the repulsive branch. The points of attachment for the small- R extension are (energies relative to the potential minimum)

$$\begin{aligned} A : \quad U(2.804259 \text{ \AA}) &= 1451.281 \text{ cm}^{-1}; \\ U(2.805916 \text{ \AA}) &= 1431.379 \text{ cm}^{-1}. \end{aligned} \quad (5)$$

For the B potential, I first used an RKR curve calculated from the constants given by Gerstenkorn and Luc,³ with smoothing of the small- R region ($<2.63 \text{ \AA}$) to remove the small RKR anomalies there. However, for this state two potentials that should be better have been published—an inverted perturbation approach (IPA) potential by Gerstenkorn *et al.*^{3,32} and the direct quantal fitting determination by Salumbides *et al.*⁵ The IPA potential tracks the RKR curve closely up to about 4250 cm^{-1} ($\nu = 60$), where the erratic behavior in the latter sets is shown in Fig. 4; however, the IPA curve does not seem to reproduce the spectroscopic energies as well as indicated in Fig. 2 of Ref. 32. For example there is a roughly constant 0.03 cm^{-1} offset between the G_ν eigenvalues and their values computed from the spectroscopic parameters. The quantal potential from Ref. 5 behaves anomalously on its repulsive branch above the high- ν limit of the data ($\nu = 43$), where the small- R extension was attached. Also, it is displaced to small R by $>0.0005 \text{ \AA}$ over the region of importance for absorption. This behavior is likely due in part to use of a nonadiabatic correction term in the centrifugal potential, which means this modification should be used in any rotational averaging of the $B \leftarrow X$ spectrum. Then it becomes

a question whether this should also be done for the A and C states. (It was deemed not necessary for the X state in Ref. 5.)

For consistency I retain the usual adiabatic centrifugal potential for all states, but I allow for various points of attachment for the small- R exponential extension of the B curve. As is discussed below, the fitting is surprisingly sensitive to this choice. My base curve is the RKR curve, as after adjustment with my attachment, this gives better spectroscopic properties than the similarly modified IPA potential. For future reference I include in Fig. 4 the effects on the B repulsive branch of these choices. Note that here an R shift of 0.0005 \AA corresponds to an energy shift of 10–15 cm^{-1} , which represents a spectral shift of 0.3 nm below 500 nm.

The quantal X potential was determined in Ref. 5 without the nonadiabatic centrifugal potential and differs from the RKR curve in the low- ν region of concern here by a negligible $\sim 10^{-5} \text{ \AA}$ in R . I have used the RKR curve computed from the constants of Martin *et al.*⁴

For the $B \rightarrow C$ predissociation calculations, I use the Gerstenkorn and Luc RKR curve for the B state. For the C potential, I use the exponential expansions and also inverse power and 6–12 forms, as have been used to treat this problem before.

C. Least-squares algorithm

The computations were designed like those used for Br_2 in Ref. 20, and were coded in double precision Microsoft FORTRAN for a PC. The algorithm included the Marquardt modification,^{33,34} which was invaluable in limiting divergence. The spectral data were treated as infinite-resolution samples; checks showed that for a 1-nm bandwidth, the observed variations in ϵ produce negligible deviations from Beer's Law for truly continuous absorption. In addition to the parameters for the potential curves, the fit model included 7 parameters for the transition moment functions, with those for $A \leftarrow X$ and $C \leftarrow X$ treated as linear functions of R but that for $B \leftarrow X$ as quadratic. To deal with the perceived systematic errors discussed earlier, wavelength shift parameters were included for both my spectra and those of Tamres and Bhat,²⁶ and intensity scaling parameters were included for my two spectra separately (to allow for possible cell temperature errors at my higher T) and for the Ref. 26 spectra collectively.³⁵ The sinusoidal wavelength correction for my spectrophotometer was adopted as determined,²⁸ though the phase factor was checked as an adjustable parameter in some computations. The final parameter was the $B \rightarrow C$ predissociation factor from Eq. (3). With allowance for 2 adjustable parameters for the A and B potentials and 6 for the C curve, the final model had 24 parameters; however, not all of these were statistically significant in the results discussed below.

As in the Br_2 study, statistical errors in the derived spectra, potential curves, and transition moment functions were computed using the full expression for error propagation, as needed for the correlated fit parameters;³⁶ all partial derivatives required here and in the fitting were evaluated numerically.

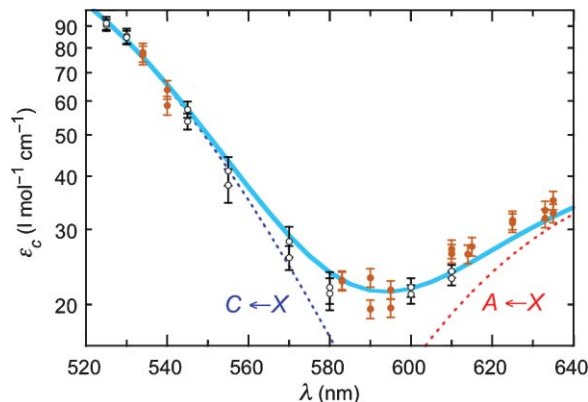


FIG. 5. Estimates of continuum absorptivity in region of discrete $B \leftarrow X$ absorption (points, Ref. 16, two sets of experiments) compared with estimates of the total (solid curve) and component bands (dashed) obtained from present analysis of spectra at two temperatures.

IV. RESULTS AND DISCUSSION

A. Preliminary analysis of absorption spectra

Initially, just the new data at two temperatures and the ϵ_c estimates from Ref. 16 were included in the analysis, for the purpose of checking consistency and testing the importance of different assumptions in the model – such as numbers of adjustable parameters needed for the potentials. Results (Fig. 5) showed that the model could accommodate the new ϵ_c data in the 525–640-nm region with only two terms in the exponential expansion for the A -state potential, one or two for B , and two or three for C , with linear transition moment functions for all three transitions. Results were also roughly consistent with the Ref. 16 determination of $|\mu_e(R)|^2$ for the $B \leftarrow X$ system (Fig. 6), justifying inclusion of these data in the fit; however, in this case the transition moment function was defined to include a term quadratic in R , to allow for deviations from the linear form over the larger range of R encompassed in the present analysis.

The early fitting showed that the transition moment slopes for the $A \leftarrow X$ and $C \leftarrow X$ systems were not well deter-

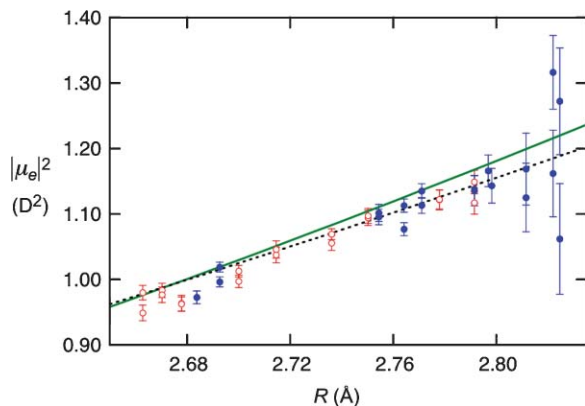


FIG. 6. $B \leftarrow X$ transition strengths from Ref. 16 (points, two sets of experiments), compared with results from present analysis for a fit model having 2, 1, and 2 adjustable parameters in Eq. (4), for the A , B , and C states, respectively. The curves represent results obtained using just the average J (solid) and averaging over 5 J levels (dashed) in the analysis of spectra at two temperatures.

mined statistically and were also sensitive to minor changes in the model. (Similar results were obtained in the earlier analysis of the Br_2 spectrum when data for only two temperatures $<30^\circ$ apart were included.²⁰) This result led me to add the data from Tamres and Bhat,²⁶ which extend to 120°C . Comparisons of these data with mine then led to the inclusion of wavelength shift and intensity scaling parameters to accommodate likely systematic errors in the different data sets.

In the effort to understand these source-dependent differences, I became aware of an instrumental problem that put my own wavelengths in doubt, even though I had previously characterized the wavelength error for this instrument in great detail.²⁸ Although these effects are still being quantified,³⁷ it is clear that the wavelength corrections depend upon a number of instrumental parameters. For the 1-nm resolution and 2-nm sampling used for my spectra, it is difficult to determine the correction from scans of atomic emission lines. Accordingly, this correction was incorporated in the analysis, giving final subtractive corrections <0.20 nm. For the Ref. 26 data, the fitting indicated a positive wavelength correction of 0.8 nm. Note that because the analysis is anchored by secure knowledge about the A and B potentials at larger R , both of these corrections can be determined by fitting.

The intensity scaling factors cannot all be determined simultaneously, because all fitted spectral quantities are proportional to one of these; thus for fixed weights, the experimental values will simply collapse to zero to reduce the minimization target, the sum of weighted squared residuals.³⁸ From preliminary examination, the Ref. 26 absorptivities were systematically larger than mine. Thus I examined results for two limiting assumptions—scale factors of 1.0 for either the Tamres and Bhat data or for my 35° data. With the former assumption, the fitted scale factor for my 35° data was 1.0045(48); with the latter, the factor for the Ref. 26 data was 0.9856(48). In both cases the scale factor for my 64° data was smaller than that for the 35° data by 0.35%. Since 35° was only 12° above room temperature, those cell temperature estimates should be more trustworthy, as mentioned earlier. Then the smaller scale factor for my 64° data translates into a -1.2° correction to that cell temperature. For the final analysis I chose to fix the scale factor for my 35° data at 1.00 and that for the Ref. 26 data at 0.99, the latter in deference to the stated precision of the mass measurements used to determine the amount of I_2 in their cell.

B. $B \rightarrow C$ predissociation

From their observations of interference effects and of very similar B -state vibrational dependence for hyperfine, rotational, and magnetic predissociation, Vigué *et al.*²⁴ concluded that all three processes involved the C state. They also found³⁹ that the 6–12 potential devised by Chapman and Bunker (CB) to explain magnetic predissociation,⁴⁰ and associated by them with a presumed 0_u^- state, better accounted for the vibrational dependence than a potential of form R^{-9} estimated by me from an early treatment of $B \rightarrow C$ spontaneous predissociation.⁴¹ My updated analysis¹⁰ of the $C \leftarrow X$ absorption replaced the R^{-9} curve with one of form

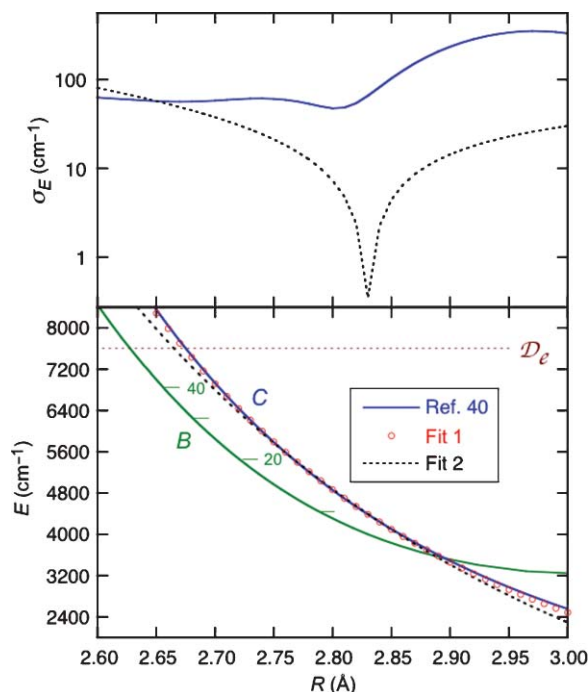


FIG. 7. I₂ B and C potentials relevant to B → C predissociation (below), and statistical error in the C potential (above). LS-fitted C curves: 1 – $U_C = -41 + 9.69 \times 10^7/R^{9.606}$; 2 – $U_C = -2155 + 6.55 \times 10^6/R^{6.64}$. Error curves (above; note logarithmic scale): solid – from spectral fitting using a 4-parameter exponential polynomial; dashed – predissociation fitting yielding curve 1. Energies are relative to the first dissociation limit. B-state vibrational levels 10–40 are shown; the B/C crossing occurs just above $\nu_B = 2$.

$R^{-9.5}$, which lies very close to the CB 6–12 curve in the relevant R region; in fact both cross the B curve only 0.0001 Å apart, near 2.896 Å and 3535 cm⁻¹ above the first dissociation limit.

The C curves obtained from the early analyses of the absorption spectra mostly agreed adequately with these two curves in the absorption region (2.6–2.8 Å), but they did not reproduce the ν_B dependence of the predissociation. In fact, when employed in precise quantal calculations of the B–C overlap integrals, even the 6–12 and 9.5 potentials did not give optimal statistical agreement with the α_ν^2 values from Table VII of Ref. 24, as could be seen from significantly improved statistics when slightly altered versions of these were used. These observations led me to code the problem for least-squares optimization, from which the most instructive result was the remarkable precision of the fitted C potential near 2.83 Å, illustrated in Fig. 7. It was this result that led me to take this as the reference distance R_0 for the C state in Eq. (4). Note that this distance is 0.07 Å smaller than R at the B/C crossing. (The average R value, or R centroid, is the crossing R .)

A second surprise from the predissociation fitting was finding two different local LS minima when an inverse-power form was used for the C potential. These are the two fitted C curves illustrated in Fig. 7, and their performance in reproducing the rates is illustrated in Fig. 8. One of these curves lies very close to the CB 6–12 potential; but in fact the other yields the better fit. However, even the latter χ^2 value is too large, having a probability <0.001 for the 18 degrees of freedom in

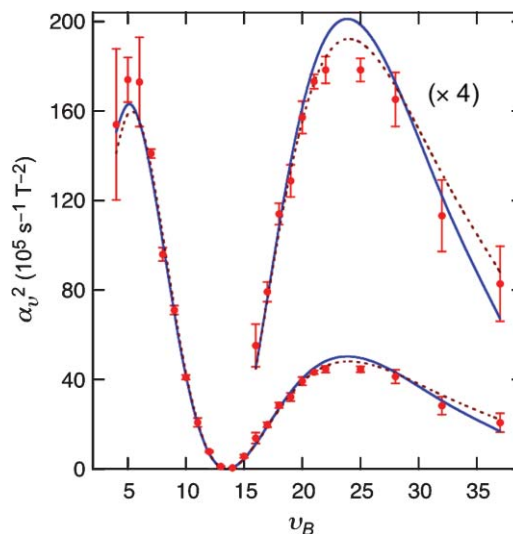


FIG. 8. Rate coefficients for magnetic predissociation from Ref. 24 and fitted results from C potential curves 1 (solid) and 2 (dashed) shown in Fig. 7. For large ν_B , where the rate data represent a range of levels, the errors have been expanded to include the effect of the ν_B uncertainty. The two fits gave reduced χ^2 values of 4.04 (solid) and 2.89.

this fit.⁴² This is perhaps a consequence of overly optimistic statistical errors in the α_ν^2 values, or limitations in the model used to obtain them. On the other hand, it could indicate that a second final state participates weakly in the predissociation. This possibility is discussed further below.

Only the first LS-fitted C curve in Fig. 7 resembles the results from the spectral fitting. Efforts to meld this curve with the best from the spectral fitting proved frustratingly difficult, so I coded for simultaneous LS analysis of both the spectral and the predissociation data. At the same time I added 8 points on the repulsive branch of the RKR curve for the C-state well, as was noted earlier. This approach succeeded, yielding final predissociative rate factors close to those shown (solid curve) in Fig. 8.

C. Dependence on B-state point of attachment

As was noted in conjunction with Fig. 4, the LS χ^2 showed a clear dependence on the point of attachment of the exponential B extension to the RKR curve, dropping monotonically by 4.5% as the attachment point was lowered from $\nu = 46$ to $\nu \approx 35$, and then stabilizing. The resulting B potential, after adjustment to preserve the RKR widths,²² actually displays better quantum mechanical reliability than the RKR curve, as is illustrated in Fig. 9. However, it still gives rotational energies exceeding the experimental values by as much as ~ 0.05 cm⁻¹ at the upper data limits of ν and J , so cannot be considered adequate. A full direct-potential analysis of the B state data is beyond the scope of the present work. However, it is useful to indicate the sensitivity of the fitting to the attachment point, as this constitutes an assumption of the model.

Changes in the attachment point for the B potential most significantly affect the transition moment functions for $B \leftarrow X$ and $C \leftarrow X$ and the estimated $C \leftarrow X$ spectrum. Figure 10 shows that the differences in the latter exceed

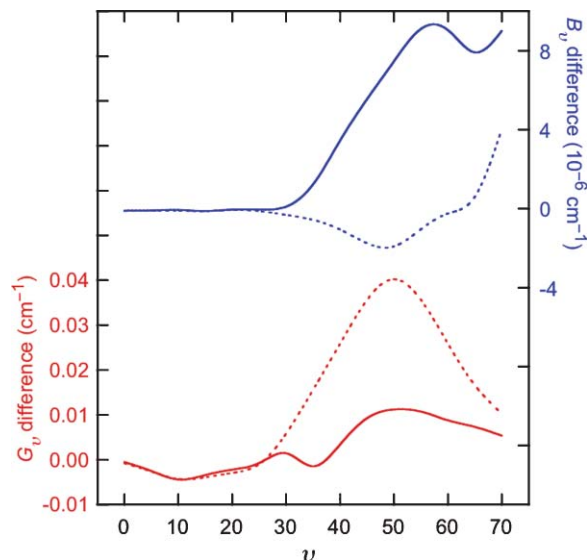


FIG. 9. Quantal properties of RKR B -state potential (dashed) and its modification as obtained from spectral fitting with exponential polynomial attached at $v = 33$ (solid). Plotted quantities are computed – spectroscopic. The combined vibrational and rotational energy excesses are comparable for the two curves at high v and the upper limit of the J data field in Ref. 3. (The RKR curve is smoothed above $v = 61$ with a potential of form $1/R$,¹³ as indicated by its behavior at smaller v .)

the statistical error; they are compensated by changes in the $B \leftarrow X$ spectrum that preserve the greater precision of the total spectrum. The transition moment function for $B \leftarrow X$ has a statistically significant quadratic component for the higher attachment but is adequately linear for the statistically best fit (Fig. 11). The slope of the $C \leftarrow X$ moment function changes sign for the same change in potentials. The negative sign is consistent with behavior observed for Br_2 (Refs. 17 and 20) and predicted theoretically for I_2 ,⁴³ however, this slope is only marginally determined in the best fit and smaller in magnitude than estimated from theory. The $B \leftarrow X$ transition moment is

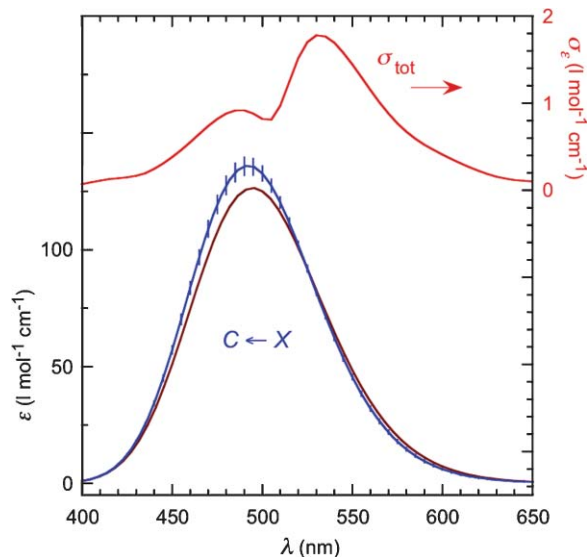


FIG. 10. Computed $C \leftarrow X$ spectra for attachment of the small- R extension of the B potential at $v = 33$ (with $1\text{-}\sigma$ error bars) and at $v = 46$; and the uncertainty (1σ) in the total spectrum (scale right).

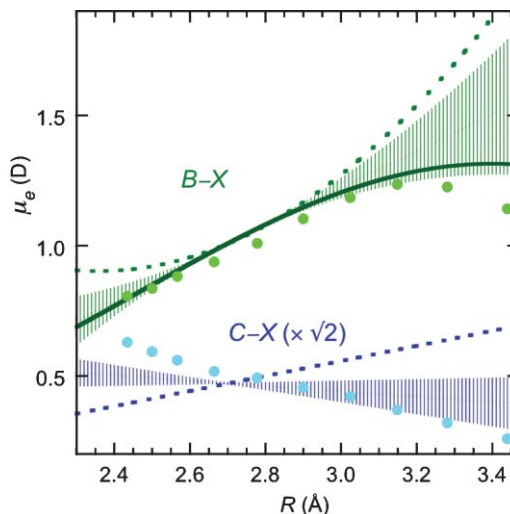


FIG. 11. Electronic transition moment functions for the $B \leftarrow X$ and $C \leftarrow X$ transitions. Broken curves represent results obtained attaching the B extension at $v = 46$. Points are theoretical estimates from Ref. 43. The solid curve for $B \leftarrow X$ is from Ref. 16. Error bars (shading) are 1σ .

of course very well defined in the region of strong absorption, where it is pinned down by the precise results from Ref. 16; the best-fit results remain consistent with the latter at larger R . The model error in the B and C potential curves exceeds the statistical error in the absorption region, but beyond the B/C crossing, the C potential is less sensitive to the attachment point (Fig. 12). The A state and its properties (not illustrated) are much less sensitive to the point of attachment of the B

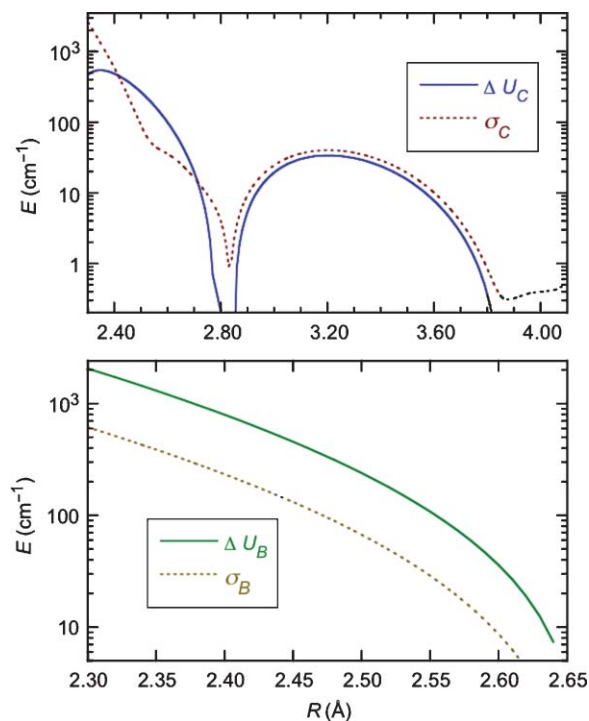


FIG. 12. Model error (ΔU) and statistical error in B and C potential curves. The ΔU values are the differences between results obtained attaching the small- R B extension at $v = 46$ and at $v = 33$, in the sense $U_{46} - U_{33}$. The statistical error in the B potential vanishes at the point of attachment to the RKR curve, as the latter is treated as error-free.

TABLE I. Least-squares analysis of I₂ visible absorption and *B*-state predissociation.^a

Parameter ^{a,b}	<i>A</i>	<i>B</i> ^c	<i>C</i>
<i>A</i> ₀	−226.70	−1783.226	−211.0 (2.5)
<i>B</i> ₀	3401.305	4408.223	4599.3 (2.5)
<i>a</i> ₁	−6.36(17)	−4.63 (11)	−3.297 (23)
<i>a</i> ₂	−4.0 (1.1)		0.505 (49)
<i>a</i> ₃			−0.46 (11)
<i>a</i> ₅ ^d			−0.33 (7)
<i>μ</i> ₀ ^e	0.2845 (11)	1.0055 (12)	0.4714 (32)
<i>μ</i> ₁ ^e	−0.048 (33)	0.72 (3)	−0.16 (11)
<i>μ</i> ₂		−0.17 (42)	
<i>χ</i> _v ²		1.186	

^aPotential curve parameters as defined in Eq. (4), with *R*₀ = 2.7 for the *A* and *B* states, 2.83 for *C*; transition moment functions defined as $|\mu_e| = \mu_0 + \mu_1 z + \mu_2 z^2$, with $z = (R - 2.7)$.

^bStandard errors in parentheses, in terms of final digits. Units cm^{−1}, Å, and debye, with energies defined relative to state *T*_e values (*A* and *B*) or dissociation asymptote (*C*). Other parameters: wavelength corrections (additive, nm)—−0.14(7) for present data and 0.80(9) for Ref. 26; intensity scale factors—1.00 for present data at 35 °C and 0.99 for Ref. 26 (both fixed), and 0.9963(8) for 64 °C. All parameters have been rounded systematically to preserve accuracy (Ref. 44).

^cPredissociative rate coefficient (*P* in Eq. (3)) = 3.22(3) × 10¹⁰ s^{−1} T^{−2}.

^dNote absence of fourth-order term, which was dropped for statistical insignificance; the original fitted value was −0.07(94).

^eTransition moments fitted for assumed nondegenerate transitions. With allowance for electronic degeneracy (*G*_{ab} in Eq. (1)), the values of *μ*₀ and *μ*₁ for the *A*–*X* and *C*–*X* systems should be divided by $\sqrt{2}$.

extension, so their statistical errors adequately encompass the uncertainties.

D. Recommended results

The results from the fit with the *B*-state extension attached at *v* = 33 are given in Table I, and the corresponding computed spectrum is given in Table II for two temperatures, to aid in interpolating for other temperatures in this approximate range. (The component bands are available in the supplementary material.²⁵) The error plotted in Fig. 10 is a guide to the statistical reliability of these results, but it should be augmented by ~0.5% in recognition of remaining intensity scale uncertainties. Also, these results are from the pseudocontinuum model for the *B* state, so they are not easily related to experimental observations in the 500–630-nm region, where discrete vibrational structure remains prominent at quite low resolution, even when the rotational lines are sufficiently pressure-broadened to render Beer's Law applicable at low-to-moderate resolution (0.1–1 nm); treating such structure requires a different approach.^{16,45}

In addition to the data already discussed and used in the present analysis, there have been several recent attempts to measure ϵ precisely in the region $\lambda \leq 500$ nm, stimulated in part by increased interest in measuring atmospheric I₂.^{45–48} The most precise of these is 572 ± 6 l mol^{−1} cm^{−1} at 500 nm from Spietz *et al.*,⁴⁵ which is significantly below the present room-*T* estimate (590 ± 4 l mol^{−1} cm^{−1}). The values at this wavelength from Saiz-Lopez *et al.*⁴⁷ (599) and Bauer *et al.*⁴⁸ (588) agree with mine. However, their estimates at 436 nm—40.0 (Ref. 47) and 36.9 ± 1.3 (Ref. 48) lie above my calculated room-*T* value (31.0 ± 0.4). In fact, the cross sec-

TABLE II. Computed molar absorptivity (l mol^{−1} cm^{−1}) of I₂(g) at 0 °C and at 35 °C.^a

λ (nm)	0 °C		35 °C		λ (nm)	0 °C		35 °C	
	0 °C	35 °C	0 °C	35 °C		0 °C	35 °C	0 °C	35 °C
390	0.18	0.28	565	405.54	415.96	740	24.04	24.06	
395	0.37	0.56	570	345.89	361.42	745	22.13	22.34	
400	0.73	1.05	575	291.04	310.35	750	20.28	20.65	
405	1.38	1.89	580	242.13	263.84	755	18.50	19.02	
410	2.47	3.29	585	199.56	222.44	760	16.80	17.45	
415	4.27	5.49	590	163.45	186.41	765	15.19	15.95	
420	7.08	8.83	595	133.52	155.69	770	13.69	14.53	
425	11.34	13.73	600	109.30	130.01	775	12.29	13.20	
430	17.52	20.69	605	90.14	108.95	780	10.99	11.95	
435	26.22	30.24	610	75.36	92.02	785	9.79	10.78	
440	38.07	43.02	615	64.28	78.68	790	8.70	9.70	
445	53.78	59.66	620	56.23	68.39	795	7.70	8.70	
450	74.08	80.85	625	50.60	60.62	800	6.79	7.79	
455	99.74	107.28	630	46.84	54.87	805	5.98	6.95	
460	131.49	139.57	635	44.51	50.74	810	5.25	6.19	
465	170.00	178.24	640	43.21	47.86	815	4.59	5.50	
470	215.71	223.55	645	42.62	45.89	820	4.01	4.87	
475	268.73	275.37	650	42.47	44.59	825	3.49	4.31	
480	328.57	332.99	655	42.57	43.71	830	3.03	3.80	
485	394.05	395.08	660	42.75	43.08	835	2.63	3.35	
490	463.20	459.63	665	42.88	42.58	840	2.27	2.94	
495	533.16	523.97	670	42.92	42.13	845	1.96	2.58	
500	600.45	584.98	675	42.76	41.63	850	1.69	2.26	
505	661.21	639.36	680	42.37	41.00	855	1.45	1.98	
510	711.99	684.29	685	41.75	40.23	860	1.25	1.73	
515	749.65	717.30	690	40.91	39.33	865	1.07	1.51	
520	772.28	737.03	695	39.83	38.26	870	0.92	1.32	
525	778.42	742.43	700	38.55	37.07	875	0.79	1.15	
530	768.32	733.85	705	37.09	35.73	880	0.67	1.00	
535	742.51	711.76	710	35.45	34.25	885	0.57	0.87	
540	703.36	678.15	715	33.66	32.64	890	0.49	0.75	
545	653.11	634.77	720	31.81	30.98	895	0.42	0.65	
550	595.24	584.47	725	29.89	29.27	900	0.35	0.57	
555	532.61	529.50	730	27.94	27.53				
560	468.56	472.66	735	25.98	25.79				

^aIndividual component bands provided as supplementary material (Ref. 25).

tion provided as a supplement to Ref. 47 lies uniformly about 10 l mol^{−1} cm^{−1} above my 35 °C spectrum for the entire region 400–485 nm; at long wavelengths it drops to zero near 740 nm, largely missing the *A* ← *X* shoulder in this region.

To the extent that there is a wavelength where ϵ is independent of temperature, it appears to be 487 nm for temperatures near room *T*, rather than 480, as claimed previously for ~100 °C.²⁶ My two computed spectra intersect there, with $\epsilon = 416$ l mol^{−1} cm^{−1}.

As was noted previously (Fig. 1), the *A* ← *X* spectrum and the small-*R* extension for the *A* potential curve have changed little since my 1982 report. The analysis was actually presented earlier, in conjunction with a first estimated RKR potential for the *A* state.⁴⁹ More precise comparisons show that at the current point of attachment of the extension (Eq. (5)) the 1981 curve lies 0.006 Å to smaller *R*, placing it ~80 cm^{−1} lower at that *R*. However, the current exponential extension and the previous *R*^{−11} curve agree within the

current statistical error for $R = 2.43\text{--}2.73 \text{ \AA}$, and differ by at most 30 cm^{-1} in the range $2.53\text{--}2.76 \text{ \AA}$.

For the predissociation data, the final fit yielded a sum of weighted squared residuals slightly below that for the first fitted C potential in Fig. 7, but still $\sim 50\%$ higher than obtained for a C potential not constrained by the spectral data or the RKR points at large R . The pattern of residuals is similar to that for the solid curve in Fig. 8—a computed shortfall at small ν , an excess in the $\nu = 20\text{--}30$ region, with largest discrepancies at $\nu = 7$ (-4.3σ) and 25 (3.9σ). Of the other states that might augment $B \rightarrow C$ predissociation, the 0_u^- originally invoked by Chapman and Bunker⁴⁰ is now fairly well known at larger R , where it lies well above the A state but below C .^{50,51} Theoretical calculations place it just to the left of the B curve at smaller R ,⁵² where it could increase the computed predissociative decay at high ν ; however that is in the wrong direction to reduce the residuals in Fig. 8. Other candidate states for B -state predissociation are even less well known, so more detailed consideration of their possible roles seems unwarranted at this time. Regarding the systematic differences between experimental and computed rates, recall that the three analyzed processes did not all yield perfectly scalable ν_B dependence, with the rate coefficients for rotational predissociation showing the clearest discrepancies.²⁴ This behavior was attributed to a strong R -dependence in the electronic matrix element from a near-cancellation of two contributing terms, an explanation that is only partly supported by more recent theory.⁵³ On the other hand, other experiments have yielded higher estimates of the hyperfine and rotational predissociation rates in the $\nu_B = 17\text{--}25$ range,⁵⁴ largely removing the special discrepancies there. My attempts to explain the smaller systematic disparities in the magnetic rates by including an R -dependent electronic matrix element have been to no avail; however, these efforts have been limited to linear functions of R , and it is possible that narrow peaked functions might have a more significant effect, as they do in other predissociations.⁵⁵

The large residuals for the predissociation data account for about half of the excess in χ_ν^2 for the analysis (Table I), relative to its expected value of unity. A residuals plot for the spectral data can be found in the supplementary material.²⁵

V. CONCLUSION

Absorption spectra of I_2 are recorded with high quantitative precision at 1-nm resolution over the spectral range 400–850 nm, and together with other spectral and predissociation data, are analyzed by least-squares using quantum calculations of the required Franck-Condon matrix elements. The results yield an improved resolution of the spectrum into its three electronic transitions and better estimates of the small- R regions of the A , B , and C potential curves. For purely continuous absorption at $\lambda \leq 500 \text{ nm}$, the fitted molar absorptivity at $35 \text{ }^\circ\text{C}$ and its calculated counterpart at $0 \text{ }^\circ\text{C}$ should now be reliable within $\sim 0.5\%$, but full realization of such precision requires wavelength accuracy better than 0.2 nm . The electronic transition moment function for the $B \leftarrow X$ tran-

sition is very well determined, thanks to inclusion of precise results for it from a different recent analysis. For the $A \leftarrow X$ and $C \leftarrow X$ systems, the moment function shows a negative slope, in agreement with theoretical predictions; however, the slope is only barely determined statistically, and for the $C \leftarrow X$ transition is subject to model error, being clearly positive if the small- R extension of the B curve is attached to the latter's RKR curve at higher ν . In this connection, certain limitations and inconsistencies in the B potential are pointed out and discussed.

The new description of the C -state potential extends to its van der Waals well at $R > 4 \text{ \AA}$ and through the B -state predissociation data, is especially precise (1 cm^{-1}) at 2.83 \AA , which is 0.07 \AA below its crossing with the B potential curve. However, the fit of the predissociation data is not statistically adequate, raising questions about the data and the possibility that the C state may not be totally responsible for the predissociation. In the spectral analysis, the $C \leftarrow X$ transition is the most changed quantity, the most significant difference being its 18% smaller integrated intensity.

The method used for this analysis was established in principle 35 years ago¹⁷ and could have been used for the present analysis shortly thereafter, when the precise predissociation data became available. Its present implementation has been facilitated by the ease of collecting abundant, precise spectrophotometric data with instrumentation that has been available for at least 20 years. The R -dependence of the transition moment functions is the least well-determined quantity, a deficiency I attribute to the limited temperature range of the spectra. The analysis is greatly facilitated by precise knowledge of two of the three required upper potential curves at larger R , from discrete spectroscopy. It remains to be seen how well the method can handle solution spectra,² where such information is lacking.

¹R. S. Mulliken, *J. Chem. Phys.* **55**, 288 (1971).

²The C state has often been labeled B'' , but C is strongly recommended, for consistency with the same states in Cl_2 and Br_2 . The use of different labeling in I_2 is an unfortunate historical accident; see R. I. Gray, K. M. Lockett, and J. Tellinghuisen, *J. Phys. Chem. A* **105**, 11183 (2001).

³S. Gerstenkorn and P. Luc, *J. Phys. (France)* **46**, 867 (1985).

⁴F. Martin, R. Bacis, S. Churassy, and J. Vergès, *J. Mol. Spectrosc.* **116**, 71 (1986).

⁵E. J. Salumbides, K. S. E. Eikema, W. Ubachs, U. Hollenstein, H. Knöckel, and E. Tiemann, *Eur. Phys. J. D* **47**, 171 (2008).

⁶D. R. T. Appadoo, R. J. Le Roy, P. F. Bernath, S. Gerstenkorn, P. Luc, J. Vergès, J. Sinzelle, J. Chevillard, and Y. D'Aignaux, *J. Chem. Phys.* **104**, 903 (1996).

⁷J. Tellinghuisen, *J. Chem. Phys.* **118**, 3532 (2003).

⁸J. Tellinghuisen, *J. Chem. Phys.* **82**, 4012 (1985).

⁹D. Inard, D. Cerny, M. Nota, R. Bacis, S. Churassy, and V. Skorokhodov, *Chem. Phys.* **243**, 305 (1999).

¹⁰J. Tellinghuisen, *J. Chem. Phys.* **76**, 4736 (1982).

¹¹J. Tellinghuisen, *J. Chem. Phys.* **58**, 2821 (1973).

¹²J. Tellinghuisen, *J. Chem. Phys.* **59**, 849 (1973).

¹³R. J. Oldman, R. K. Sander, and K. R. Wilson, *J. Chem. Phys.* **54**, 4127 (1971).

¹⁴J. R. Wiesenfeld and R. H. Young, *Chem. Phys.* **58**, 51 (1981).

¹⁵S. J. Davis, *Appl. Phys. Lett.* **32**, 656 (1978).

¹⁶J. Tellinghuisen, *J. Chem. Phys.* **134**, 084301 (2011).

¹⁷R. J. Le Roy, R. G. Macdonald, and G. Burns, *J. Chem. Phys.* **65**, 1485 (1976).

¹⁸A. A. Passchier, J. D. Christian, and N. W. Gregory, *J. Phys. Chem.* **71**, 937 (1967).

¹⁹J. B. Burkholder and E. J. Bair, *J. Phys. Chem.* **87**, 1859 (1983).

- ²⁰J. Tellinghuisen, *J. Chem. Phys.* **115**, 10417 (2001); J. Tellinghuisen, *ibid.* **118**, 1573 (2003).
- ²¹J. Tellinghuisen, *J. Chem. Phys.* **80**, 5472 (1984).
- ²²J. Tellinghuisen, *Adv. Chem. Phys.* **60**, 299 (1985).
- ²³D. A. Chestakov, D. H. Parker, K. V. Vidma, and T. P. Rakitzis, *J. Chem. Phys.* **124**, 024315 (2006).
- ²⁴J. Vigué, M. Broyer, and J. C. Lehmann, *J. Phys.* **42**, 961 (1981).
- ²⁵See supplementary material at <http://dx.doi.org/10.1063/1.3616039> for the spectral data and other information. Note that at the 1-nm resolution of these spectra, vibrational structure is still evident in the 600–650-nm region. However, the present data, sampled every 2 nm, represent near averages of the local ε values, hence are suitable for analysis with the pseudo-continuum model. This assumption was tested in the fitting by deletion of the points in this region, with little effect on the results other than loss of precision from the reduced number of data points.
- ²⁶M. Tamres and S. N. Bhat, *J. Phys. Chem.* **75**, 1057 (1971).
- ²⁷F. T. Lang and R. L. Strong, *J. Am. Chem. Soc.* **87**, 2345 (1965).
- ²⁸J. Tellinghuisen, *Appl. Spectrosc.* **54**, 1208 (2000).
- ²⁹B. H. Wells, E. B. Smith, and R. N. Zare, *Chem. Phys. Lett.* **99**, 244 (1983).
- ³⁰J. Tellinghuisen, *J. Mol. Spectrosc.* **141**, 258 (1990).
- ³¹The computed bound-free absorption is insensitive to the actual dissociation limit, provided the potential curve is smooth and the continuum wavefunctions are properly energy normalized; see Ref. 22 and J. Tellinghuisen, *Can. J. Chem.* **82**, 826 (2004).
- ³²S. Gerstenkorn, P. Luc, and C. Amiot, *J. Phys. (France)* **46**, 355 (1985).
- ³³D. W. Marquardt, *J. Soc. Ind. Appl. Math.* **11**, 431 (1963).
- ³⁴W. H. Press, B. P. Flannery, S. A. Teukolsky, and W. T. Vetterling, *Numerical Recipes*, (Cambridge University Press, Cambridge, England, 1986).
- ³⁵The scale factor for the 35° spectra was also applied to the ε_e and $|\mu_e(R)|^2$ values from Ref. 16, since these were based on data from the same instrument.
- ³⁶J. Tellinghuisen, *J. Phys. Chem. A* **105**, 3917 (2001).
- ³⁷J. Tellinghuisen (unpublished).
- ³⁸If such scale factors are associated with the computed rather than the measured spectra, they become indeterminate through correlation with the parameters defining the transition moment functions.
- ³⁹J. Vigué, M. Broyer, and J. C. Lehmann, *J. Phys.* **42**, 949 (1981).
- ⁴⁰G. D. Chapman and P. R. Bunker, *J. Chem. Phys.* **57**, 2951 (1972).
- ⁴¹J. Tellinghuisen, *J. Chem. Phys.* **57**, 2397 (1972).
- ⁴²P. R. Bevington, *Data Reduction and Error Analysis for the Physical Sciences* (McGraw-Hill, New York, 1969).
- ⁴³A. Zaitsevskii, E. A. Pazyuk, A. V. Stolyarov, Ch. Teichteil, and V. Vallet, *Mol. Phys.* **98**, 1973 (2000).
- ⁴⁴J. Tellinghuisen, *J. Mol. Spectrosc.* **137**, 248 (1989).
- ⁴⁵P. Spietz, J. G. Martin, and J. P. Burrows, *Atmos. Chem. Phys.* **6**, 2177 (2006).
- ⁴⁶A. Saiz-Lopez and J. M. C. Plane, *Geophys. Res. Lett.* **31**, L04112 (2004).
- ⁴⁷A. Saiz-Lopez, R. W. Saunders, D. M. Joseph, S. H. Ashworth, and J. M. C. Plane, *Atmos. Chem. Phys.* **4**, 1443 (2004).
- ⁴⁸D. Bauer, T. Ingham, S. A. Carl, G. K. Moortgat, and J. N. Crowley, *J. Phys. Chem. A* **102**, 2857 (1998).
- ⁴⁹K. S. Viswanathan, A. Sur, and J. Tellinghuisen, *J. Molec. Spectrosc.* **86**, 393 (1981).
- ⁵⁰J. Tellinghuisen, *Can. J. Chem.* **71**, 1645 (1993).
- ⁵¹S. Motohiro, S. Nakajima, K. Aoyama, E. Kagi, H. Fujiwara, M. Fukushima, and T. Ishiwata, *J. Chem. Phys.* **117**, 9777 (2002).
- ⁵²W. A. de Jong, L. Visscher, and W. C. Nieuwpoort, *J. Chem. Phys.* **107**, 9046 (1997).
- ⁵³E. A. Pazyuk, A. V. Stolyarov, V. I. Pupyshev, N. F. Stepanov, S. Ya Uman-skii, and A. A. Buchachenko, *Mol. Phys.* **99**, 91 (2001).
- ⁵⁴E. Martínez, M. T. Martínez, and F. Castaño, *J. Molec. Spectrosc.* **128**, 554 (1988).
- ⁵⁵A. L. Roche and J. Tellinghuisen, *Mol. Phys.* **38**, 129 (1979).